Saccharinate-Based Ionic Liquids and Lithium Battery Electrolytes

Batteries & Supercaps

Research Article
doi.org/10.1002/batt.202400758

Chemistry Europe
European Chemical Societies Publishing

www.batteries-supercaps.org

Saccharinate-Based Ionic Liquids and Lithium Battery Electrolytes

Mukhtiar Ahmed,[a] Ashok Kushwaha,[a] Andrei Filippov,[a] Patrik Johansson,*[b, c] and Faiz Ullah Shah*[a]

Fluorine-free ionic liquids (ILs) and electrolytes based on ether-functionalized pyrrolidinium or imidazolinium cations coupled with a "greener", non-basic, and hydrolytically stable saccharinate (Sac) anion, are herein presented with their thermal, transport and electrochemical properties. The thermal stability, glass transition temperature, and electrochemical stability of the imidazolinium based ILs surpasses the pyrrolidinium IL, while the latter offer better (ion) transport properties. Ether-functionalization of the IL cation improves the transport properties with negligible effects on the thermal and electrochemical stabilities. The Li^+ conducting electrolytes – created by adding 10 mol% of lithium saccharinate (LiSac) to the neat (BMMIm)(Sac) and (C_{201}MMIm)(Sac) ILs show an as low initial overpotential as ± 0.05 V and outstanding Li stripping/plating performance over 100 hours at 60 °C for the latter, but a very large polarization interfacial resistance, 4730 Ω cm^2, impeding the kinetics of stripping/plating, even at these elevated temperatures for the former. Hence the rather modest modification has an enormous impact in practice.

Introduction

The increasing societal demand for electric vehicles is driving the development of efficient batteries with higher energy densities and longer life beyond the capabilities of current lithium-ion batteries (LIBs).[1] This evolution is particularly significant in the exploration of advanced battery technologies such as lithium metal, lithium–sulfur (Li–S), and also multivalent batteries, that can potentially provide higher energy density, using a metal anode. Although, lithium metal electrodes, offer very low negative potentials (−3.05 V vs. SHE) and an exceptionally high specific capacity (~3860 mAh g^{-1}), such batteries face critical challenges, often originating in insufficient electrolyte/electrode interfacial stability.[2,3] Electrolyte engineering is thus crucial and yet no silver bullet has been found.

In stark contrast, today's state-of-the-art LIB electrolytes, such as LP30 comprising 1 M lithium hexafluorophosphate ($LiPF_6$) in a 1:1 ratio of ethylene carbonate (EC) and dimethyl carbonate (DMC), are flammable and the heavily fluorinated $LiPF_6$ salt may disintegrate at higher temperatures,[4] producing extremely hazardous hydrofluoric acid (HF) and other toxic organophosphorus compounds.[5,6] Although it forms a stable solid electrolyte interphase (SEI) on graphite anodes,[7] it has a narrow electrochemical stability window and causes dendritic growth on lithium metal anodes. Thus, to pursue the use of lithium metal anodes, safer and non-flammable, and not the least still performant electrolytes are urgently needed.

Ionic liquids (ILs) are salts that remain liquid at temperatures below 100 °C,[8] and as some are liquid at ambient temperature, they can potentially be liquid electrolytes alternatives,[9] due to their nonvolatile nature, superior thermal stabilities, and structural diversity. The downside is the fluorinated anions used and there is a scarcity of suitable IL anions overall, commonly termed the "*anion crisis*".[10] Therefore, there is a golden opportunity to create new fluorine-free anions with the ability to form ILs with sufficiently low melting points, being non-basic and non-nucleophilic, easily synthesizable from readily available precursors, as well as being cost-effective, and thermally and hydrolytically stable.[11–13]

For the IL cation, the inclusion of an ether group is well-known to contribute to low viscosity and high ionic conductivity.[14,15] The very flexible ether chains pack less efficiently, giving more accessible free volume and thus improve transport properties.[16,17] For example, Ribeiro and co-workers proved through molecular dynamics (MD) simulations that the structural orientation and less efficient assembly of the alkoxy chains in ILs is the main reason for their lower viscosity in comparison with structurally analogous ILs having alkyl chains.[18] With respect to electrolytes, IL-based electrolytes for batteries are typically made by dissolving a lithium salt, of the same or different anion as the one in the IL – which acts as matrix/solvent. In such electrolytes, Li^+ mobility remains a key issue as the small sized Li^+ ion diffuses slower than the bulky organic cations and anions, due to the strong electrostatic

[a] M. Ahmed, A. Kushwaha, A. Filippov, F. Ullah Shah
Chemistry of Interfaces, Luleå University of Technology, SE-971 87 Luleå, Sweden
E-mail: faiz.ullah@ltu.se

[b] P. Johansson
Department of Physics, Chalmers University of Technology, -SE-412 96 Gothenburg, Sweden
E-mail: patrik.johansson@chalmers.se

[c] P. Johansson
ALISTORE-European Research Institute, FR CNRS 3104, Hub de l'Energie 15, Rue Baudelocque, -80039 Amiens, France

Supporting information for this article is available on the WWW under https://doi.org/10.1002/batt.202400758

Research Article
doi.org/10.1002/batt.202400758
Chemistry Europe
European Chemical Societies Publishing

interactions – leading to formation of ion-pairs, triplets and higher aggregates.[19,20] The ether-functionalization of the IL cation is known to weaken the interactions between Li^+ and the IL anion by providing a new site for the Li^+ to interact with,[21] resulting in a lower cation partial anion solvation number and improved rate performance.[22]

In this work, we resort on novel ILs made by coupling ether-functionalized pyrrolidinium and imidazolinium cations with a readily accessible and "greener", non-basic, and hydrolytically stable saccharinate (Sac) anion, an anion which has structural and property similarities[23,24] with well-known fluorinated anions such as bis[(trifluoromethyl)sulfonyl]imide (TFSI)[25] and 2,2,2-trifluoro-*N*-(trifluoromethylsulfonyl)acetamide (TSAC) (Figure 1).[26] Its compact aromatic structure can offer enhanced thermal and transport properties,[27,28] and the doping of these Sac-based ILs with LiSac salt renders Li^+ conducting liquid electrolytes, all of which properties studied and reported upon herein, alongside stripping/plating of Li in Li||Li symmetric cells.

Experimental

Materials and Synthesis

Unless otherwise stated, all the commercial reagents were used without any further purification. 1-methylimidazole (ACS reagents, >97% purity), 1,2-dimethylimidazole (ACS reagents, >97% purity), *n*-methylpyrrolidine (ACS reagents, >97% purity), 1-bromobutane (>99% purity), methoxyethyl bromide, lithium hydroxide monohydrate (ACS reagents, >97% purity) and saccharine (ACS reagents, >97% purity) were all received from Sigma-Aldrich. Sodium sulphate (anhydrous, 99% purity) and dichloromethane (DCM) (96% purity) were purchased from VWR (BDH) chemicals.

The synthesis and structural characterization of the ILs are provided in detail in the supporting information (SI). For electrolyte preparation, neat ILs and LiSac were dried at 50 °C under high vacuum overnight, followed by drying at 80 °C for at least 24 hours, and then transferred into an argon-filled glove box (Mbraun, Germany, with H_2O <0.5 ppm and O_2 <0.5 ppm), where 10 mol% LiSac was added in the neat ILs and the electrolytes stirred until transparent and homogenous. Prior to any measurements, the samples were kept in a vacuum oven at 80 °C for at least four days. The water contents were measured by Karl Fischer titration (using Metrohm 917 Coulometer, Switzerland) placed inside the glovebox.

Nuclear Magnetic Resonance Spectroscopy

The structures and purity of all the synthesized ILs were confirmed using a Bruker Ascend Aeon WB 400 (Bruker BioSpin AG, Fallanden, Switzerland) nuclear magnetic resonance (NMR) spectrometer with working frequencies of 400.21 MHz for ^1H and 100.64 MHz for ^{13}C. $CDCl_3$ was used as solvent and the data were processed with the Bruker Topspin 3.5 software.

Thermal Analysis

Thermogravimetric analysis (TGA) was performed using a PerkinElmer TGA 8000 under N_2 at a heating rate of 10 °C per min, and *ca.* 2–3 mg of sample for each experiment. The onset of the decomposition temperature (T_d) was calculated using the Pyris software from the intersection of the baseline weight and the tangent of the weight vs. temperature curve. Differential scanning calorimetry (DSC), both cooling and heating traces, was carried out using a PerkinElmer DSC 6000 with *ca.* 2–4 mg of sample placed in an aluminium pan, and at a scan rate of 5 °C min^{-1}, under constant flow of dry N_2 gas at a rate of 20 mL min^{-1}. The glass transition temperature (T_g) was determined from the inflection mid-point of the initial *S*-shaped transition slope using the Pyris software.

Electrochemical Characterization

The electrochemical stabilities and ionic conductivities were both determined using a Metrohm Autolab PGSTAT302N electrochemical workstation with a FRA32M module for impedance measurements, all controlled by a Nova 2.02 software. A sealed Microcell HC from rhd instruments Germany was used to hold about 70 μL of the liquid sample. To determine the electrochemical stability window (ESW), linear sweep voltammetry (LSV) was performed with a three-electrode setup: a glassy carbon (GC) working electrode (WE), a Pt crucible as the counter electrode (CE) as well as a sample container, and an Ag wire coated with AgCl as a pseudo-reference electrode (RE). Both cathodic and anodic scans were recorded at a rate of 1 mV s^{-1}. The electrochemical potentials were calibrated using ferrocene (Fc) as an internal reference and shifted using $E_{Li/Li^+} \approx$

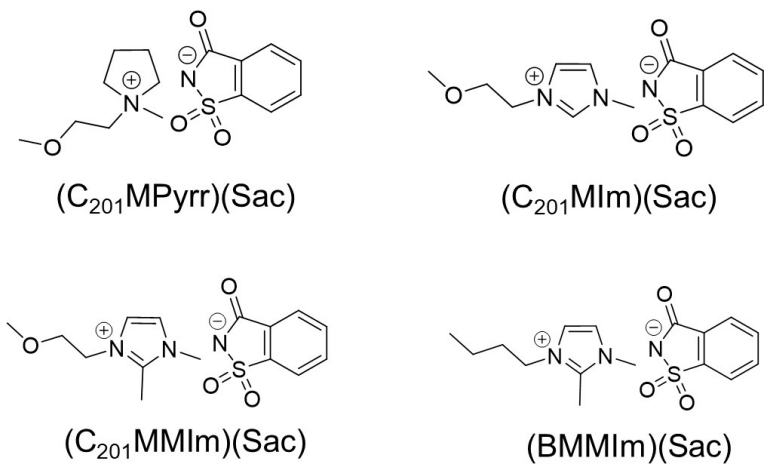

Figure 1. Structures and acronyms of the ILs.

$E_{Fc/Fc^+} + 3.2$ V.[29] The ESWs limits were defined by a 0.1 mA cm^{-2} cut-off current density.

The ionic conductivities were further analyzed by fitting the data to the Vogel-Fulcher-Tammann (VFT) equation, (Equation (1)):[30]

$$\sigma = \sigma_0 \exp\left(\frac{-B}{(T - T_0)}\right) \quad (1)$$

where σ_0 is a pre-exponential factor, B is an empirical material-dependent fitting parameter related to the dynamic T_g and activation/pseudo activation energy (E_σ) of the system. The reference temperature T_0 is attributed to the ideal vitreous transition temperature, at which configurational entropy vanishes. T_0 is determined by fitting the temperature-dependent ionic conductivity data to the VTF equation.

Prior to each LSV and ionic conductivity measurement, the electrodes were polished with a 0.25 m of Kemet diamond paste. The cell was thermally equilibrated for 10 minutes before recording the impedance spectra. The cell constant was calculated using a Metrohm 100 μS cm^{-1} KCl standard solution ($K_{cell} = 18.5396$ cm^{-1}).

Cell Fabrication

Li|Li symmetrical cells were assembled using CR2032 coin cell cases, 14 mm diameter lithium (Li) metal foil electrodes (a soft-bristled toothbrush was used to brush the oxide film of the Li foil), glass fiber separators (GF/A) (Cytiva, 260 μm), and 80 μL of electrolyte. Electrochemical impedance spectroscopy (EIS) was performed by applying a frequency range from 1 MHz to 10 mHz, with a 5 mV sinusoidal amplitude. The Li|LFP cell was assembled following a similar method. The lithium iron phosphate (LFP) electrode was prepared using a doctor blade technique. The LFP served as the active material, Super P carbon black as the conductive agent, and polyvinylidene fluoride (PVDF) as the binder, all mixed using a weight ratio of 80:10:10. The mixture was dispersed in *N*-methyl-2-pyrrolidone (NMP) solvent to form a slurry, which was then uniformly coated onto an aluminum current collector. The coated electrode was dried in a vacuum oven at 90 °C for 12 hours, after which it was cut into circular electrodes with a diameter of 14 mm. All measurements were conducted using a VMP-3 BioLogic instrument.

NMR Diffusometry

Pulsed field gradient (PFG) NMR diffusometry measurements of diffusion coefficients[31] were performed using a Bruker Ascend/Aeon WB 400 (Bruker BioSpin AG) NMR spectrometer with a resonance frequency of 400.21 MHz for ^{1}H and 155.56 MHz for ^{7}Li. The PFG NMR measurements were performed with a PFG NMR probe Diff50 (Bruker) with a maximum amplitude of the magnetic field gradient pulse of 29.73 T m^{-1}. The samples were placed in a standard 5 mm NMR glass tube and closed with a plastic stopper to avoid contact with air. Prior to measurements, each sample was equilibrated at the specific temperature for at least 20 min. The diffusivity is obtained from the diffusion decay (DD) of amplitude *A* of NMR spectral line, obtained by Fourier transformation of a descending half of stimulated-echo (StE), as a function of the amplitude of applied pulsed field gradient. For the StE pulse sequence used, the DD of *A* in the case of a simple non-associated molecular liquid, can be described by Equation (2):[31]

$$A(g, \delta, t_d) = A(0) \exp(-\gamma^2 g^2 \delta^2 D t_d) \quad (2)$$

where A(0) is the factor proportional to the magnetic nuclei content in the system, and to spin-lattice and spin-spin relaxation times, γ is the gyromagnetic ratio for a used nucleus; g and δ are the amplitude and duration of the gradient pulse; t_d is the diffusion time; and D is the self-diffusion coefficient. t_d was in the range 4–100 ms for ^{1}H diffusion and 5–15 ms for ^{7}Li diffusion. No diffusion time dependence was observed in these measurements.

The diffusivity data for the ILs and electrolytes were analyzed using the VFT Equation (3):

$$D = D_0 \exp\left(\frac{-B}{(T - T_0)}\right) \quad (3)$$

where D_0, T_0, B are adjustable parameters. The activation energy for diffusion (E_D) is related to B as $E_D = B \times R$. We have described $D(T)$ by fitting D_0, T_0 and B.

Results and Discussion

We start with the synthesis and structural characterization of ILs and electrolytes, which is followed by the assessment of their thermal properties, and finally conclude with more battery-related properties, such as ionic conductivity and electrochemical stabilities as well as stripping/plating tests using a Li||Li symmetric and a full Li||LFP cell. The synthesis, TGA, DSC and LSV data for (BMMIm)(Sac) have recently been reported by some of us[24] and will therefore not be described nor discussed in detail, but its transport properties are discussed for comparison purposes.

Synthesis and Structural Characterization

The synthesis of the ILs is carried out in two steps. In the first step, ether functionalized imidazolinium and pyrrolidinium bromide salts are created *via* a direct quaternization reaction between methoxyethyl bromide and the corresponding charge neutral heterocyclic amines.[32,33] The reaction is exothermic and completed in few minutes with a high yield, >90%. Low temperature, slight excess of the methoxyethyl bromide, and absence of oxygen significantly increase the overall yield. In the second step, a metathesis of the bromide salts with sodium saccharine in aqueous media is carried out and this results in the desired ILs with good yields (*ca.* 75–80%). All the synthesized ILs are liquid at ambient temperature.

Water is a pervasive impurity in ILs, capable of being absorbed by both hydrophilic and hydrophobic systems, and thus profoundly impacts the key physicochemical properties such as ionic conductivity, ion diffusion and electrochemical stability. Elevated water content reduces viscosity and thereby facilitating enhanced mass transport and improve ionic conductivity, but significantly narrows the ESW, primarily due to water electrolysis at both cathodic and anodic processes. For example, R.G. Compton *et al.*[34] demonstrated that vacuum-dried ILs with water content ≤200 ppm, exhibits remarkably broader ESWs compared to their moisture-laden counterparts, highlighting the critical role of water in governing IL perform-

ance. In this work, the ILs as well as the electrolytes have water content less than 105 ppm (Table 1), and has negligible impact on the key physicochemical properties.

The NMR spectroscopy data (Figures S1–6) of the synthesized ILs corroborate well with their structures and confirm their purity. First, the ether chain attached to the cation exhibits distinct ^{1}H-NMR resonance lines – the singlet for the methoxy group present at 3.2–3.3 ppm and the two triplets at *ca.* 4.0–4.6 and *ca.* 3.6–3.8 ppm for the methylene protons, which is further complemented by the ^{13}C NMR resonance lines – the methoxy carbon at *ca.* 60 ppm, while the two methylene carbons are at *ca.* 70 and 45 ppm. Second, the presence of distinct ^{1}H NMR resonance lines representing aromatic groups in the range from 7 to 8 ppm complemented with ^{13}C NMR resonance lines at 100–145 ppm and the presence of the carbonyl ^{13}C NMR resonance line at 170 ppm confirm the success of the metathesis reaction and the purity of the final products.

Thermal Properties

All the ILs display a one-step thermal decomposition, and the weight loss occurs within the temperature range 250–350 °C, indicating that the cation and the anion decompose more or less at the same temperature (Figure 2a, Table 1). Yet, the thermal stabilities assessed by dynamic TGA are overestimated and should be truly quantitatively established by isothermal TGA analysis.[35,36] The thermal stability of the imidazolium-based ILs is better than the pyrrolidinium-based ILs, and even further increases for the C-2 methylated imidazolium-based IL. This is due to the relatively higher thermal stability of the imidazolinium cation and by prevention of the carbene formation.[37] The ether functionalization of the imidazolium cation has almost no effect on the thermal stability. Changing from organic cation to Li^{+}, *i.e.* from IL to Li-salt, the thermal stability increases by over 100 °C, suggesting stronger ionic interactions and an aromatically stabilized $(Sac)^{-}$ anion and the same is true for the electrolytes. Overall, the thermal stabilities of these ILs and electrolytes are on par with previously reported fluorine-free ILs,[38,39] and most notably, they exhibit superior thermal stability compared to organic LIB electrolytes, such as LP30, which decompose at temperatures well below 100 °C.[4]

The DSC traces confirmed all the ILs to be glass formers and no other thermal events are observed in the studied temperature range (Figure 2b). The imidazolium- ILs show higher T_g than their pyrrolidinium analogues (Table 1), which can be attributed to the stronger π–π and dispersion interactions – high ionic strength/ ion-ion interaction and, thus, higher thermal energy is required to reach the same ionic mobility as for pyrrolidinium-based ILs.[40] The incorporation of an ether

Table 1. Physico-chemical and electrochemical properties.[a]

System	Water content (±5 ppm)	T_g (°C)	T_d (°C)	σ at 30 °C (S cm^{-1})	ESW (V)
(C_{201}Pyrr)(Sac)	105	−60	256	1.2×10^{-3}	2.8
(C_{201}MIm)(Sac)	98	−49	203	4.9×10^{-4}	4.3
(C_{201}MMIm)(Sac)	84	−47	320	1.4×10^{-4}	4.3
$[(C_{201}MMIm)(Sac)]_{0.9}[(Li)(Sac)]_{0.1}$	94	−45	336	3.4×10^{-5}	4.5
$[(BMMIm)(Sac)]_{0.9}[(Li)(Sac)]_{0.1}$	78	−28	327	4.1×10^{-6}	4.7

a = T_g: glass transition temperature, T_d: decomposition temperature, σ: ionic conductivity.

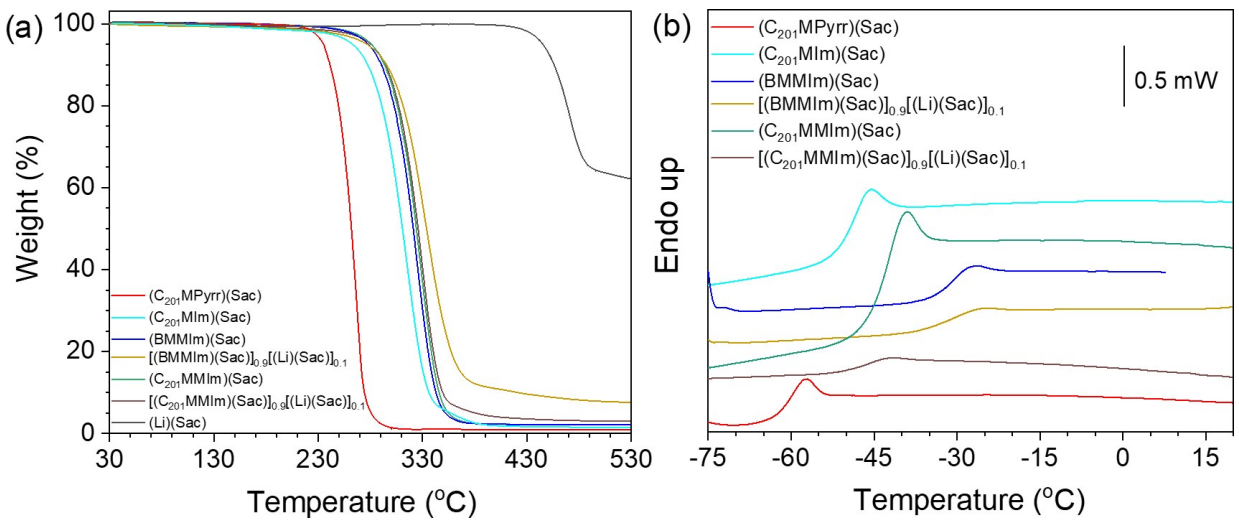

Figure 2. TGA thermographs: neat ILs, electrolytes and LiSac (a) and DSC traces: neat ILs and electrolytes (b). All traces are shifted along the Y-axis for clarity. Data for (BMMIm)(Sac) are reproduced with permission from [24].

Research Article
doi.org/10.1002/batt.202400758
Chemistry Europe
European Chemical Societies Publishing

moiety into the cation structures lowers the T_g [24] due to the larger structural flexibility, reduced symmetry of the cations, and the repulsive interactions induced by the lone pairs of electrons on the oxygen atoms of the neighboring -OR units – all together hinder crystallization/melting processes,[13] and lower the lattice energy.[41] As expected, doping the ILs with a Li salt slightly increase their T_g, and is attributed to the stronger ionic interactions and aggregate formation.

Ionic Conductivity

As expected, the ionic conductivities of the ILs and the electrolytes increase with increasing temperature (Figure 3). The (C_{201}MPyrr)(Sac) exhibit higher ionic conductivities at lower temperatures than the imidazolium analogues (Table 1), however, its ionic conductivities converge with [(C_{201}MIm)(Sac)] and remain comparable at higher temperatures. This is attributed to the relatively stronger Coulombic and vdW interactions at lower temperatures, together with the possibility of molecular aggregate formation below 50 °C.[42,43] Although the methyl group at the C-2 position of the imidazolium ring improves its chemical stability,[44] the ionic conductivity is reduced due to the larger cation size and increased noncovalent interactions. Yet, ether functionalization of the imidazolium ring increases the ionic conductivity of the IL, which is due to the decreased the ionic interactions, which corroborates well with the DSC data as well as with the literature.[45,46]

Turning to the electrolytes, doping the ILs with Li-salts reduces the ionic conductivity,[16] which can be linked to increased ionic interactions, aggregate formation and reduced free volume. The differences in ionic conductivity are larger at lower temperatures, again indicating robust ionic interactions and aggregate formation at lower temperatures and reduced at elevated temperatures.[42]

The VFT data shows slightly lower activation energy for the pyrrolidinium-based IL (Table S1), and higher for the electrolytes, which corroborates well with the DSC data. The T_0 values for all ILs and electrolytes fall in the range 160–198 K and are in good agreement with the calorimetric T_g as obtained by DSC.

Ion Diffusivity

To better comprehend the transport properties at molecular level and acquire deeper insights into the relative mobility of ions, ^{1}H and ^{7}Li PFG NMR diffusometry was employed. As expected, the diffusion coefficients of all the ions exhibit a monotonous increase as a function of temperature and follow VFT trends (Figure 4a). Among the ILs, both the ions of (C_{201}MPyrr)(Sac) diffuse faster at lower temperatures compared to its imidazolium analogues but this difference dies out at higher temperatures – which again corroborates well with the DSC and ionic conductivity data. For all ILs, the Sac anion diffuses slightly slower as compared to the cations and this difference is a bit larger for (C_{201}MPyrr)(Sac), clearly indicating the role of ion size and ionic interactions. The latter is important as the diffusion measured by PFG NMR is an average of the diffusion coefficients of isolated, paired, and aggregated ions, regardless of charge, and aggregates are expected to be less mobile due to their larger size and thus decrease the average. This is in contrast to the ionic conductivity values, which primarily are determined by the mobilities of charged species.[47]

As expected, the diffusivities are reduced in both the electrolytes, the Sac anion being affected more than the organic cations, and despite the smallest radius, the Li^+ diffuses the slowest – again suggesting aggregate formation due to Li^+–Sac interactions (Figures 4b and 4c). The Li^+ diffuses somewhat faster in $[(C_{201}MMIm)(Sac)]_{0.9}[(Li)(Sac)]_{0.1}$ as compared to $[(BMMIm)(Sac)]_{0.9}[(Li)(Sac)]_{0.1}$ (Figure 7d) which agrees well with its higher ionic conductivity.

The VFT fits (Equation (3), Table S2) of the diffusion data suggest the apparent activation energy (E_D) to be higher for the

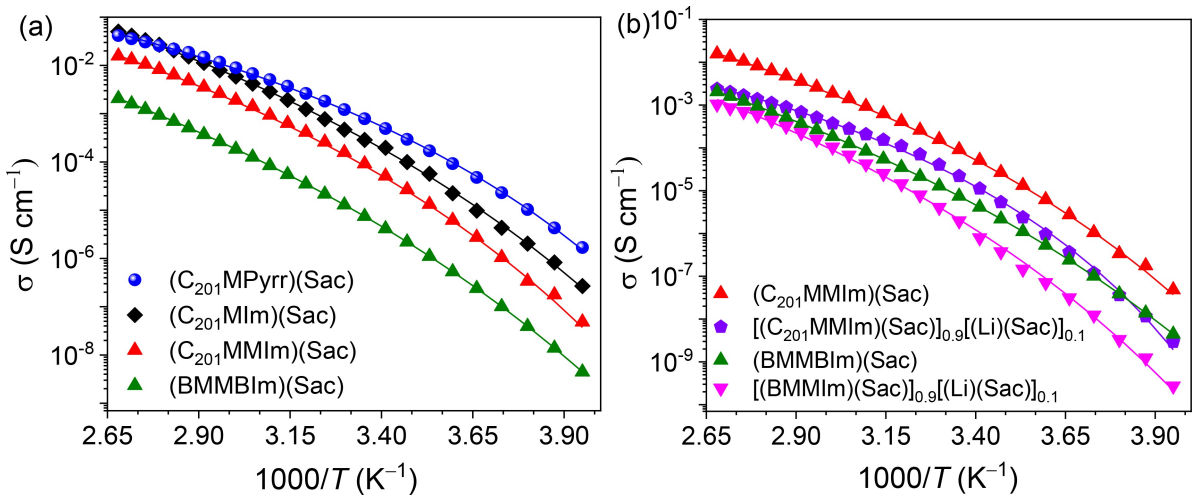

Figure 3. Ionic conductivities of the neat ILs (a), and the electrolytes, data for the corresponding neat ILs are added for the clarity (b) as function of temperature. The solid lines indicate best fit of the data to the VFT equation.

Research Article
doi.org/10.1002/batt.202400758
Chemistry Europe
European Chemical Societies Publishing

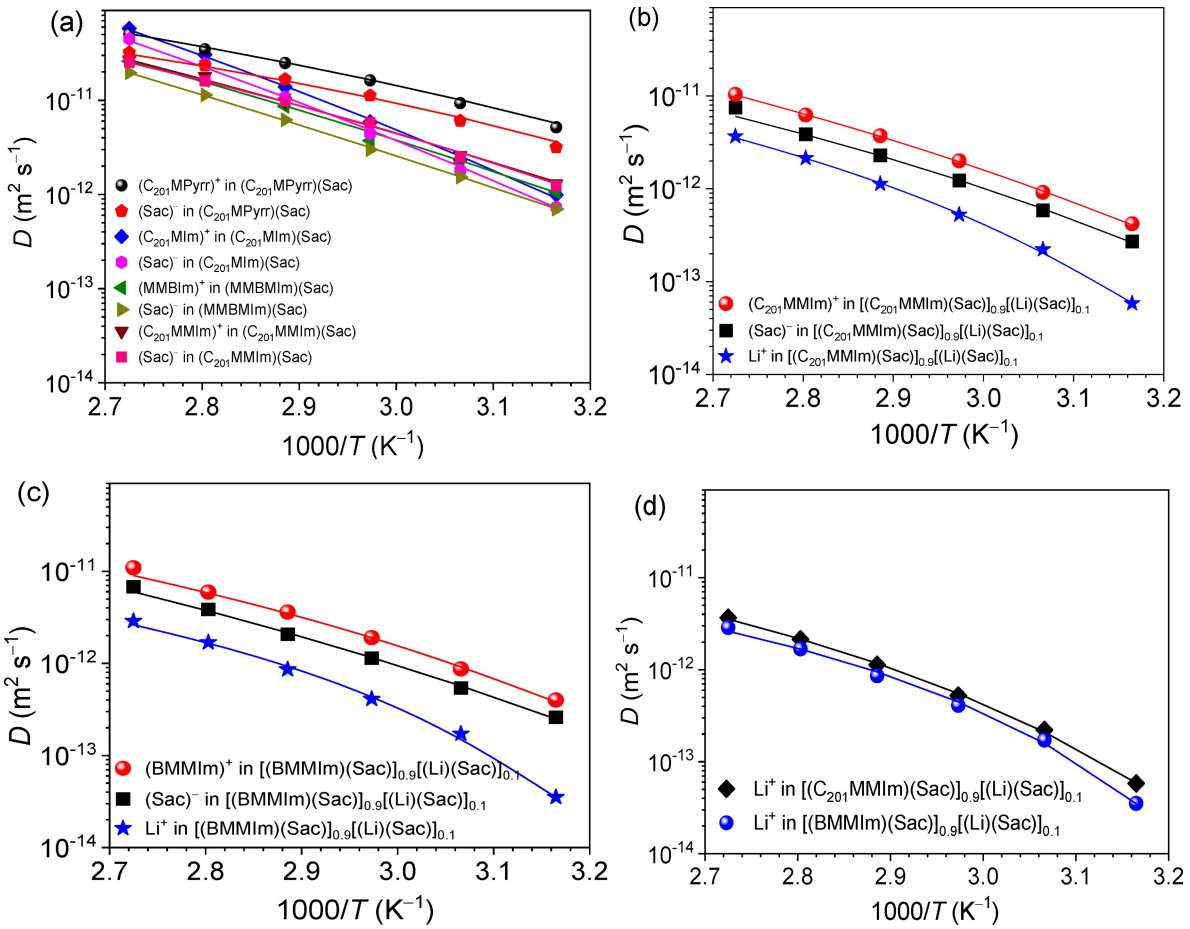

Figure 4. Diffusion coefficients for the neat ILs (a), and the ILs and the electrolytes by ^{1}H (b, c), and ^{7}Li (d) NMR spectroscopy. Symbols indicate experimental data and the solid lines are the VFT fits.

Sac anion as compared to the cations, and also higher for the imidazolinium cations than the pyrrolidinium cation, which is associated with the free volume. The T_0 for the ionic conductivity data is lower than for the diffusivity data;[48,49] again with origin in what actually is probed.

The apparent transference numbers (t_i) for each ion in the electrolytes were calculated from their diffusion coefficients (D_i) using Equation (4):[50]

$$t_i = \frac{x_i D_i}{\Sigma_i x_i D_i} \quad (4)$$

where x_i is the molar fraction of each ion. In both electrolytes the cation has higher transference numbers as compared to the Sac anion and the Li^+ cation (Figure 5). These values are most probably underestimated due to neutral aggregate formation with lower mobility, which thus not reflects the true contribution to the ionic conductivity.[51]

Electrochemical Assessments

Starting with the anodic scans of the ILs, there is an abrupt increase in current density at *ca.* 4.2 V *vs* $Li^+/Li°$ associated with oxidative decomposition for (C_{201}MPyrr)(Sac), while for (C_{201}MMIm)(Sac) and (C_{201}MIm)(Sac) it remains constant until *ca.* 5.1 *vs* $Li^+/Li°$ (Figure 6). A similar trend is observed during the cathodic scans, the (C_{201}MPyrr)(Sac) IL reduces at a lower potential than its imidazolium analogues, implying that the ESWs of the imidazolium-based ILs are wider than for the pyrrolidinium-based IL (Table 1). Incorporating the methyl group at the C-2 position on the imidazolium cation increases its reductive stability, and this agrees well with the literature on imidazolium-phosphate ILs.[52] The ESWs of the electrolytes are marginally improved, which might be due to the creation of a passivating layer on the surface of the WE.[53,54] Two separate peaks (C1 and C2) at 0.6 and 1.0 *vs* $Li^+/Li°$ are observed during the cathodic sweep of $[(C_{201}MMIm)(Sac)]_{0.9}[(Li)(Sac)]_{0.1}$, indicating underpotential deposition (UPD) of the lithium as well as possibly partial breakdown of the imidazolium cation on the GC electrode.[55] The creation of the UPD layer can passivate the surface GC electrode, which is helpful for the cathodic limit of the electrolyte, acting similarly to an SEI.

Research Article
doi.org/10.1002/batt.202400758
Chemistry Europe
European Chemical Societies Publishing

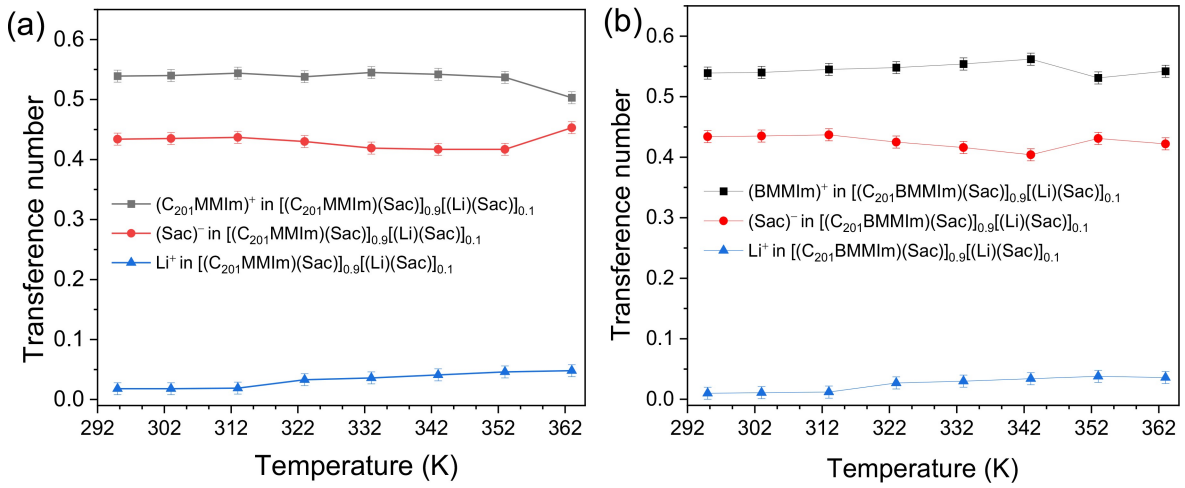

Figure 5. Apparent transference numbers in $[(C_{201}MMIm)(Sac)]_{0.9}[(Li)(Sac)]_{0.1}$ (a) and $[(BMMIm)(Sac)]_{0.9}[(Li)(Sac)]_{0.1}$ (b) as obtained from the PFG NMR diffusion data.

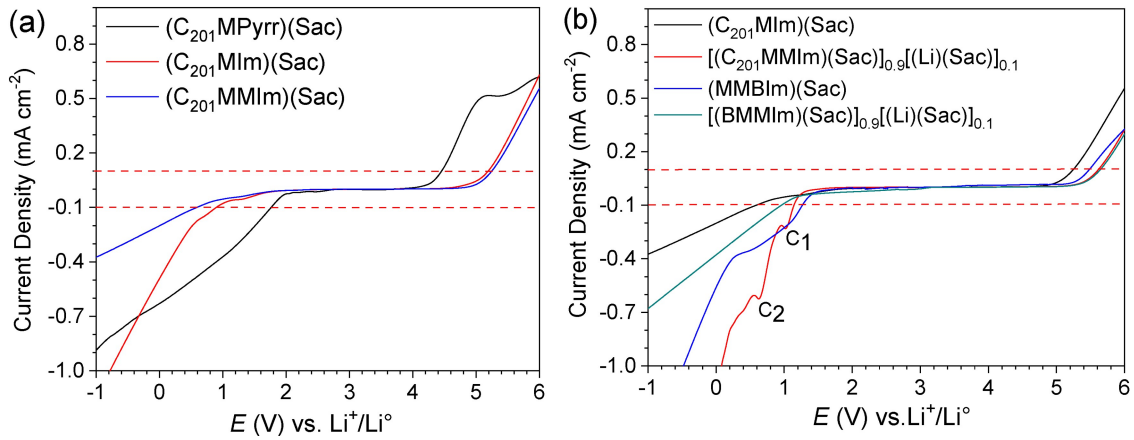

Figure 6. LSV of the neat ILs, (a) and the ILs as well as electrolytes (b), at 20 °C using GC as WE.

Turning to the compatibility of the electrolytes with Li metal anodes, the voltage profile of the Li|$[(C_{201}MMIm)(Sac)]_{0.9}[(Li)(Sac)]_{0.1}$|Li cell's stripping/plating behavior over *ca.* 100 hours exhibits an initial polarization of ±0.05 V, which gradually increased to ±0.11 V over 70 hours of stripping/plating cycles (Figure 7a). This indicates buildup of interfacial charge resistance and/or decomposition of the electrolyte. The insets magnify the voltage profile during the first 10 hours

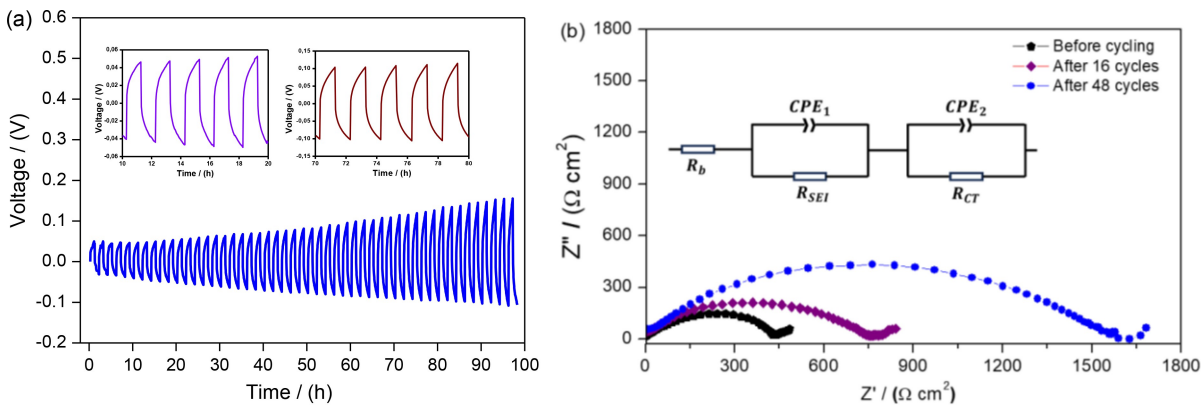

Figure 7. (a) The voltage-time profile of the Li|$[(C_{201}MMIm)(Sac)]_{0.9}[(Li)(Sac)]_{0.1}$|Li cell at 60 °C, including magnified views of the initial and final 10 hours of stripping/plating cycles at a current rate of 0.05 mA/cm^2 for 1 hour per cycle, and (b) Nyquist plots of the cell for initial and subsequent cycle numbers, illustrating the evolution of impedance with cycling.

and the last 10 hours, demonstrating a symmetric and stable electrode/electrolyte interface throughout (Figure 7a). In contrast, the LiI[(BMMIm)(Sac)]$_{0.9}$[(Li)(Sac)]$_{0.1}$|Li cell has a much higher polarization interfacial resistance, *ca.* 4730 Ω cm^2 before cycling (Figure S7), which can be attributed to a nonuniform layer formed during the rest time, due to the lower ionic conductivity and sticky nature of this electrolyte, not favoring the formation of any uniform and thin layer. This impedes the kinetics of Li^+ during stripping/plating, even at higher temperatures.

The EIS spectra of the LiI[(C_{201}MMIm)(Sac)]$_{0.9}$[(Li)(Sac)]$_{0.1}$|Li cell with the equivalent circuit chosen (Figure 7b), representing the overall interfacial resistance by the SEI resistance (R_{SEI}) and charge transfer resistance (R_{CT}). Before cycling, the interfacial resistance is lower, *ca.* 480 Ω cm^2, after resting in contact with the electrolyte for 6 hours at the open-circuit voltage (OCV), but after 16 cycles of stripping and plating, *ca.* 795 Ω cm^2, indicating decomposition of the electrolyte and continuous SEI formation. The impedance continues to increase with additional cycles and reached *ca.* 1620 Ω cm^2 after 48 cycles.

The galvanostatic charge-discharge cycling performance of the LFP cell using the [(C_{201}MMIm)(Sac)]$_{0.9}$[(Li)(Sac)]$_{0.1}$ electrolyte with a current rate of 0.1 C within the 2.5–3.8 V potential range at 60 °C showed a low specific capacity of 11.6 mAh g^{-1} and decreased further with additional cycles (Figure S8a). This relatively poor performance can be attributed to the formation of an inhomogeneous and loose lithium deposition and higher viscosity – promoting the Li-anion complexes formation and as a result hinders Li^+ transport.[56,57] In addition, the higher viscosity of an electrolyte adversely affect wettability and limit the active area of the electrode and increases the interfacial resistance.[12] The EIS analysis of this cell highlights the buildup of cell impedance with cycling. Thus, the cell exhibits higher interfacial resistance even before cycling, which further increases slightly after ten cycles due to the continuous SEI formation and electrolyte decomposition (Figure S8b). However, this does not mean that these IL-based electrolytes are not suitable for battery applications. In fact, further battery studies are required to achieve the best performance and to identify the best combination of electrode-electrolyte systems.

Conclusions

Among these ILs, imidazolium ILs offers beneficial thermal and electrochemical stabilities but higher glass transition, T_g, temperatures, and lower (ionic) transport properties. For imidazolium ILs, cation flexibility improves the transport properties but reduces electrochemical stabilities, which improved together with thermal stability for Li^+ conducting electrolytes – created by doping 10% LiSac in neat ILs – but reduced transport properties which is anticipated due to aggregate formation as Li^+ being smallest in size still diffuses slowest among the ions. The electrolyte with ether side chain revealed beneficial ion conduction and Li^+ transference number, as well as stable lithium stripping/plating behavior at 60 °C. Altogether this study suggests a way forward for designing fluorine-free and greener electrolytes for lithium metal batteries.

Acknowledgements

The financial support from the Swedish Energy Agency (project number: 48194-1) is gratefully acknowledged and PJ is grateful for the financial support from his Swedish Research Council (VR) Distinguished Professor grant 'Next Generation Batteries' (#2021-00613).

Conflict of Interests

The authors declare no conflict of interest.

Data Availability Statement

The data that support the findings of this study are available in the supplementary material of this article.

Keywords: Saccharine · Ionic liquids · Ion transport · Electrochemistry · Lithium battery electrolytes

[1] A. Colmenar-Santos, A.-M. Muñoz-Gómez, E. Rosales-Asensio, Á. López-Rey, *Energy* **2019**, *183*, 61–74.
[2] J. Després, S. Mima, A. Kitous, P. Criqui, N. Hadjsaid, I. Noirot, *Energy Econ* **2017**, *64*, 638–650.
[3] F. Mwasilu, J. J. Justo, E.-K. Kim, T. D. Do, J.-W. Jung, *Renewable Sustain. Energy Rev.* **2014**, *34*, 501–516.
[4] T. Kawamura, Yamaki, *J Power Sourc.* **2006**, *156*, 547–554.
[5] S. Lux, I. Lucas, E. Pollak, S. Passerini, M. Winter, R. Kostecki, *Electrochem. Commun.* **2012**, *14*, 47–50.
[6] A. Masias, J. Marcicki, W. A. Paxton, *ACS Energy Lett.* **2021**, *6*, 621–630.
[7] H. Ota, Y. Sakata, A. Inoue, S. Yamaguchi, *J Electrochem. Soc.* **2004**, *151*, A1659.
[8] S. A. Forsyth, J. M. Pringle, D. R. MacFarlane, *Austr. J Chem.* **2004**, *57*, 113–119.
[9] M. Moreno, E. Simonetti, G. B. Appetecchi, M. Carewska, M. Montanino, G.-T. Kim, N. Loeffler, S. Passerini, *J Electrochem. Soc.* **2016**, *164*, A6026.
[10] B. D. Rabideau, K. N. West, J. H. Davis, *Chemical Commun.* **2018**, *54*, 5019–5031.
[11] S. Bhowmick, G. Tatrari, A. Filippov, P. Johansson, F. U. Shah, *Phys. Chem.Chemical Physics* **2023**, ***25***, 19815–19823.
[12] S. Bhowmick, M. Ahmed, A. Filippov, L. C. Loaiza, F. U. Shah, P. Johansson, *Chemical Commun.* **2023**, *59*, 2620–2623.
[13] I. A. Khan, O. I. Gnezdilov, A. Filippov, F. U. Shah, *ACS Sustain. Chem. Eng.* **2021**, *9*, 7769–7780.
[14] S. Ferrari, E. Quartarone, C. Tomasi, D. Ravelli, S. Protti, M. Fagnoni, P. Mustarelli, *J Power Sour.* **2013**, *235*, 142–147.
[15] N. Terasawa, S. Tsuzuki, T. Umecky, Y. Saito, H. Matsumoto, *Chem. Commun* **2010**, *46*, 1730–1732.
[16] F. Philippi, D. Rauber, B. Kuttich, T. Kraus, C. W. Kay, R. Hempelmann, P. A. Hunt, T. Welton, *Phys. Chem. Chem. Phys.* **2020**, *22*, 23038–23056.
[17] A. Warrington, C. S. Kang, C. Forsyth, C. M. Doherty, D. Acharya, L. A. O'Dell, N. Sirigiri, J. W. Boyle, O. E. Hutt, M. Forsyth, *Mater. Chem. Front.* **2022**, *6*, 1437–1455.
[18] L. J. Siqueira, M. C. Ribeiro, *J Phys. Chem. B* **2009**, *113*, 1074–1079.
[19] M. Ahmed, S. Bhowmick, A. Filippov, P. Johansson, F. U. Shah, *Chem.–A Euro. J* **2023**, *29*, e202301000.
[20] M. Ahmed, S. S. Rao, A. Filippov, P. Johansson, F. U. Shah, *Phys.Chem. Chem.Phys.* **2023**, *25*, 3502–3512.

[21] M. Shimizu, K. Yamaguchi, H. Usui, N. Ieuji, T. Yamashita, T. Komura, Y. Domi, T. Nokami, T. Itoh, H. Sakaguchi, *J Electrochem. Soc.* **2020**, *167*, 070516.
[22] K. Shigenobu, K. Dokko, M. Watanabe, K. Ueno, *Phys. Chem. Chem.Phys.* **2020**, *22*, 15214–15221.
[23] E. B. Carter, S. L. Culver, P. A. Fox, R. D. Goode, I. Ntai, M. D. Tickell, R. K. Traylor, W. Hoffman, J. H. Davis Jr, *Chemical Commun.* **2004**, 630–631.
[24] M. Ahmed, G. Tatrari, P. Johansson, F. U. Shah, *ACS Sustain. Chem. Eng.* **2024**, *12*, 16896–16904.
[25] O. Borodin, W. Gorecki, G. D. Smith, M. Armand, *The J Phys. Chem. B* **2010**, *114*, 6786–6798.
[26] H. Matsumoto, H. Kageyama, Y. Miyazaki, *ECS Proceedings Volumes* **2002**, 1057.
[27] M. Armand, P. Johansson, *J Power Sour* **2008**, *178*, 821–825.
[28] M. Armand, P. Johansson, M. Bukowska, P. Szczeciński, L. Niedzicki, M. Marcinek, M. Dranka, J. Zachara, G. Żukowska, M. Marczewski, *J Electrochem. Soc.* **2020**, *167*, 070562.
[29] A. R. Neale, S. Murphy, P. Goodrich, C. Hardacre, J. Jacquemin, *ChemPhysChem* **2017**, *18*, 2040–2057.
[30] I. Bandrés, D. F. Montano, I. Gascón, P. Cea, C. Lafuente, *Electrochimica Acta* **2010**, *55*, 2252–2257.
[31] J. E. Tanner, *J Chem. Phys.* **1970**, *52*, 2523–2526.
[32] S. Fang, Z. Zhang, Y. Jin, L. Yang, Hirano, K. Tachibana, S. Katayama, *J Power Sources* **2011**, *196*, 5637–5644.
[33] Z. Fei, W. H. Ang, D. Zhao, R. Scopelliti, E. E. Zvereva, S. A. Katsyuba, P. J. Dyson, *J Phys. Chem. B* **2007**, ***111***, 10095–10108.
[34] A. M. O'Mahony, D. S. Silvester, L. Aldous, C. Hardacre, R. G. Compton, *J Chem. Eng. Data* **2008**, *53*, 2884.
[35] F. U. Shah, I. A. Khan, P. Johansson, *Molecules* **2020**, *25*, 2388.
[36] S. Jeong, S. Li, G. B. Appetecchi, S. Passerini, *Energy Storage Mater.* **2019**, *18*, 1–9.
[37] O. Kühl, *Chem. Soc. Rev.* **2007**, *36*, 592–607.
[38] N. Schopper, J. Landmann, J. A. Sprenger, L. Zapf, R. Bertermann, N. V. Ignat'ev, M. Finze, *Chemistry–A Euro. J* **2023**, *29*, e202301497.
[39] M. Ahmed, A. Filippov, P. Johansson, F. U. Shah, *ChemPhysChem* **2024**, *25*, e202300810.
[40] M. Kunze, S. Jeong, E. Paillard, M. Winter, S. Passerini, *J Phys. Chem. C* **2010**, *114*, 12364–12369.
[41] P. M. Dean, J. M. Pringle, D. R. MacFarlane, *Phys. Chem. Chem. Phys* **2010**, *12*, 9144–9153.
[42] W. Zhao, Z. He, B. Z. Tang, *Nature Rev. Mater.* **2020**, *5*, 869–885.
[43] J. Łuczak, J. Hupka, J. Thöming, C. Jungnickel, *Colloids and Surfaces A: Physicochem. Eng. Aspects* **2008**, *329*, 125–133.
[44] A. Filippov, O. N. Antzutkin, F. U. Shah, *Phys. Chem. Chemical Phys.* **2019**, *21*, 22531–22538.
[45] Z. B. Zhou, H. Matsumoto, K. Tatsumi, *Chem. –A Euro. J* **2004**, *10*, 6581–6591.
[46] Y. Jin, S. Fang, M. Chai, Hirano, *Indust. Eng. Chem. Res.* **2012**, *51*, 11011–11020.
[47] H. Sato, R. Kikuchi, *J Chem. Physics* **1971**, *55*, 677–702.
[48] N. Boden, S. Leng, I. Ward, *Solid State Ionics* **1991**, *45*, 261–270.
[49] N. Stolwijk, S. Obeidi, *Electrochimica Acta* **2009**, *54*, 1645–1653.
[50] A. Brady, D. Salley, *J Am. Chem. Soc.* **1948**, *70*, 914–919.
[51] V. L. Martins, N. Sanchez-Ramirez, M. C. Ribeiro, R. M. Torresi, *Phys. Chem. Chem. Phys.* **2015**, *17*, 23041–23051.
[52] S. Bhowmick, A. Filippov, I. A. Khan, F. U. Shah, *Phys. Chem. Chem. Phys.* **2022**, *24*, 23289–23300.
[53] G. M. Girard, M. Hilder, D. Nucciarone, K. Whitbread, S. Zavorine, M. Moser, M. Forsyth, D. R. MacFarlane, P. C. Howlett, *J Phys. Chem. C* **2017**, *121*, 21087–21095.
[54] G. M. Girard, M. Hilder, N. Dupre, D. Guyomard, D. Nucciarone, K. Whitbread, S. Zavorine, M. Moser, M. Forsyth, D. R. MacFarlane, *ACS Appl. Mater. Inter.* **2018**, *10*, 6719–6729.
[55] L. Gasparotto, N. Borisenko, N. Bocchi, S. Z. El Abedin, F. Endres, *Phys. Chem. Chemical Phys* **2009**, *11*, 11140–11145.
[56] X. Liu, A. Mariani, H. Adenusi, S. Passerini, *Angewandte Chemie Int. Edition* **2023**, *62*, e202219318.
[57] X. Gao, F. Wu, A. Mariani, S. Passerini, *ChemSusChem* **2019**, *12*, 4185.

Manuscript received: November 29, 2024
Revised manuscript received: January 28, 2025
Accepted manuscript online: January 29, 2025
Version of record online: February 9, 2025